Int J Mech Mater Des
DOI 10.1007/s10999-007-9042-2

Modeling the brittle–ductile transition in ferritic steels. Part II: analysis of scatter in fracture toughness

S. J. Noronha · N. M. Ghoniem

Received: 24 May 2007 / Accepted: 19 July 2007

Abstract A dislocation simulation model has been proposed to predict the brittle–ductile transition in ferritic steels in Part I. Here we extend the model to address the problem of inherent scatter in fracture toughness measurements. We carried out a series of Monte Carlo simulations using distributions of microcracks situated on the plane of a main macrocrack. Detailed statistical analysis of the simulation results showed the following: (a) fracture is initiated at one of the microcracks whose size is at the tail of the size distribution function, and (b) the inherent scatter arises from the distribution in the size of the critical microcrack that initiates the fracture and *not* from the variation of the location of the critical microcrack. Utilizing the weakest-link theory, Weibull analysis shows good agreement with the Weibull modulus values obtained from fracture toughness measurements.

Keywords Brittle–ductile transition · Fracture toughness · Weibull analysis

1 Introduction

The microstructure of ferritic steels is inhomogeneous and fracture of these steels at brittle and semi-brittle regimes initiates from localized locations (microcracks). The fracture strength, which is controlled by the inhomogenities typically, exhibits wide dispersion. Microcracks situated in the plastic zone of macrocracks are known to play a critical and detrimental role in the fracture process. When identical specimens are tested under identical conditions, scatter in fracture toughness is observed to arise from variable size, shape, orientation and location of microcracks with respect to the main macrocrack. As mentioned in (S. J. Noronha and N. M. Ghoniem submitted), the deterministic fracture toughness values calculated represents mean values, and random deviations from these values will arise due to the inhomogeneous distribution of size and the spatial distribution of microcracks in the matrix. The scatter in toughness measurements are conventionally treated using probabilistic methods based on the weakest-link theory (Curry and Knott 1976, 1979; Beremin 1983; Wallin et al. 1984; Anderson et al. 1994). Such models either use a Weibull distribution for the probability of fracture (Beremin 1983), or end up in similar expressions starting from an assumed Poisson distribution for cleavage triggering microcraks (Wallin et al. 1984; Jayatilaka and Trustrum 1977). In the Beremin model (1983), the maximum principal stress is calculated for each volume element in the plastic zone and a probability of failure is assigned. The total probability of failure is then obtained by summing over the entire plastic zone. The cumulative probability of failure is given by

S. J. Noronha (✉) · N. M. Ghoniem
Department of Mechanical and Aerospace Engineering, University of California, Los Angeles
CA 90095-1597, USA
e-mail: silvester.noronha@areva.com

$$p_f = 1 - \exp\left\{\sum_j \left[\frac{\sigma_{1,j}}{\sigma_u}\right]^m \frac{\Delta V_j}{V_u}\right\} \quad (1)$$

where $\sigma_{1,j}$ is the maximum principal stress for each volume element ΔV_j. In these models, the stress field ahead of the crack is obtained from Finite Element solutions. Both the Weibull modulus m and the scale parameter σ_u are assumed to be characteristic material parameters, which are independent of temperature, geometry and mode of loading. The parameter V_u is a characteristic volume such that $V_u \sim 1/N_v$, where N_v is the number of critical inclusions per unit volume. Currently the parameters m and σ_u are used in this model and are obtained by best-fit to experimental data. There is very little research to ascribe physical significance to model parameters, such as the carbide particle size, strength distribution, and to relate the fracture process to the fracture and flow properties of the matrix. Here we calculate the Weibull parameters from a data set obtained using our discrete dislocation simulation model (S. J. Noronha and N. M. Ghoniem submitted), starting with randomly distributed microcracks on the plane of the main macrocrack.

In the work of Hirsch and Roberts (1997), it was found that the dislocation mobility plays a significant role in determining the transition temperature. However, the temperature dependence of the dislocation mobility alone cannot explain the BDT behavior of microstructurally complex materials, like steels (Hirsch and Roberts 1997). In the part I of this work (S. J. Noronha and N. M. Ghoniem submitted), we introduced a discrete dislocation simulation model in which the effects of crack-tip blunting and plasticity at the microcrack are incorporated. Here, we extend our model to the case where microcracks of varying sizes are distributed on the crack plane ahead of the blunted macrocrack-tip. Preliminary results based on this approach were presented in Noronha and Ghoniem (2007).

2 Calculation method

From numerous experimental studies, models and observations, it has been established that in the case of ferritic steels: (a) the matrix is quite inhomogeneous with randomly distributed precipitates (mostly carbides). These carbides crack at early stages of loading and can act as potential nuclei for triggering cleavage fracture (McMahon and Cohen 1965), (b) there exist a montonic relationship between carbide and grain sizes, see e.g. Curry and Knot (1978). It has been argued that this relation is a result of ferrite grains growing from the austenite phase by rejection of carbides. Thus if there are more ferrite nuclei (finer grains), carbides will be thinner (Knott 2000). In addition, explicit grain size dependence has not been observed for fracture toughness measurements (Chen et al. 1993), (c) it has been found that the size distribution of microcracks can be approximated by a Poisson distribution (Wallin et al. 1984; Jayatilaka and Trustrum 1977). Based on these experimental observations, the model presented here takes into account the following features:

(1) The size dependence of microcracks is treated using a distribution of microcracks on the plane of a main macrocrack. The size distribution of microcracks is assumed to follow a Poisson distribution; based on the observed fact that carbide sizes follow a Poisson distribution, and most of them crack early in the loading cycle due to the plastic deformation of the matrix (Ortner and Hippsley 1996).
(2) Microcracks are uniformly distributed on the crack plane ahead of the macrocrack.
(3) The criterion for failure is based on a cleavage crack propagating from one of these microcracks into the matrix. Plasticity at the microcrack shields the crack-tip from the external load and this will increase the stress required for crack propagation.

A schematic of the present model is shown in Fig. 1, where a semi-infinite crack (macrocrack) with microcracks ahead of it on its crack plane emits dislocations from sources near its tip. The arrays of emitted dislocations form the plastic zone of the macrocrack, which will blunt due to dislocation emission. Details of the dislocation emission, motion and crack-tip blunting implementation is described in Sect. 2 of S. J. Noronha and N. M. Ghoniem (submitted). The plastic zone developed at the macrocrack modifies the stress field ahead of it to that of an elastic-plastic material with hardening (S. J. Noronha and N. M. Ghoniem submitted). The carbide microcracks placed in this field experience a tensile

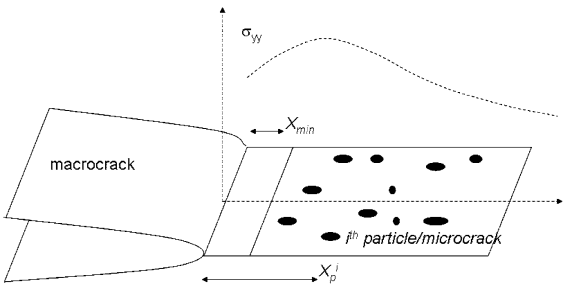

Fig. 1 The geometry of the model used: microcracks (in carbide particles) are distributed in the crack plane ahead of the macrocrack. The propagation of any of the microcracks is the failure criterion in the simulation

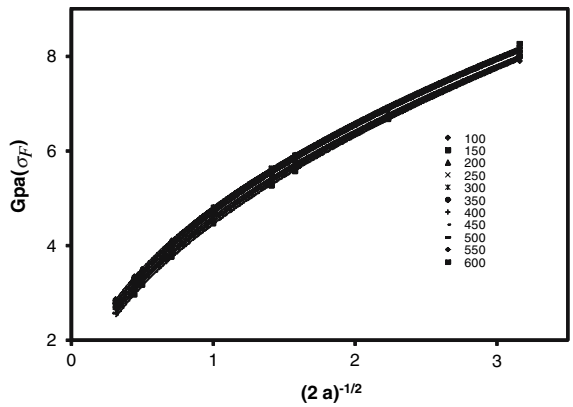

Fig. 2 The microscopic fracture stress (σ_F) as a function of the crack size (a). Different symbols indicate different friction stress (MPa) values, shown as labels

stress and are assumed to propagate, leading to fracture when the tensile stress on any of these particles reach a critical value σ_F. Simulation is done in three stages as described in detail in the following section. At first stage fracture stress of microcracks of ranging size was estimated using the methodology described in detail in Sect. 2.2 of S. J. Noronha and N. M. Ghoniem (submitted). At the second stage, the fracture stresses of microcracks of varying sizes with a Poisson distribution are estimated by interpolation of the values obtained in the preceding stage. At the final stage, the fracture thoughness is estimated by using fracture stress of microcrack distributions as fracture criterion. Thus, the applied stress intensity when normal stress at one of the microcrack ahead of the macrocrack in the crack plane reaches its predetermined value is the fracture toughness (K_F) of the sample.

3 Results and discussion

3.1 Calculation of the microscopic fracture stress (σ_F)

The microscopic fracture stress (σ_F) is estimated using procedure described in Sect. 2.2 of S. J. Noronha and N. M. Ghoniem (submitted) for a range of crack sizes, from 0.1 to 5 μm, for friction stresses ranging from 100 to 600 MPa. Figure 2 shows σ_F as a function of the inverse square root of the crack size (a). It can be seen that the relation is nearly linear for small crack sizes, but deviates for large cracks indicating the greater influence of emitted dislocations. This behavior is seen in the experimental determination of microscopic fracture stress as well (e.g. Chen et al. 1993). It should be noted that the fracture stress (σ_F) values of any given crack size calculated for different friction stress values vary marginally, and thus follows the temperature insensitivity of the microscopic fracture stress (σ_F) observed in many experiments (e.g. Bowen et al. 1987; Ortner and Hippsley 1996). From the best fit curves shown in Fig. 2, we interpolate the value of σ_F for a given crack size at any friction stress. The value of σ_F thus obtained is the critical tensile stress criterion at microcrack position used to calculate the macroscopic fracture toughness (K_F).

3.2 Generation of the microcrack distribution

To mimic the Poissonian distribution observed for the size of microcracks and carbides (Wallin et al. 1984; Jayatilaka and Trustrum 1977; Poloniecki and Wilshaw 1971), we generated microcracks with a Poisson distribution of 0.5 μm mean radius. A random number with Poisson distribution is generated using standard algorithms (Press et al. 1996) for the radius of microcracks. The fracture stress values corresponding to each of these microcracks are estimated from the interpolation of microscopic fracture stress data (in Fig. 2) and are used as input in the next stage of simulation. These microcracks are uniformly distributed in a 500 μm × 500 μm square region on the crack plane. The density of microcracks is taken to be 0.06/μm^2, comparable with the microstructure

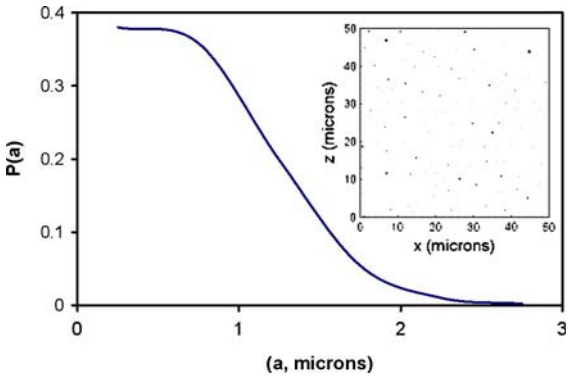

Fig. 3 Probability distribution function (PDF) of microcrack size. A Poisson distribution with mean radius of 0.5 μm is used. A plot of the spatial distribution of microcracks uniformly distributed on the crack-plane is shown in the inset

of typical steels (Curry and Knott 1979). We assume that microcracks distributed head of the main macrocrack tip are situated at a minimum distance $X_{\min}$ away from the main crack-tip. This assumption is based on the observation that finite element analysis of blunted crack-tips show that the tensile stress along the crack-plane has a maximum at about 2ρ (where ρ is the radius of curvature) from the blunted crack-tip. The distribution of a typically generated microcrack sizes is shown in Fig. 3.

3.3 Calculation of the fracture toughness (K_F)

The macrocrack is assumed to be semi-infinite with dislocation sources close to its tip. Dislocations are emitted simultaneously along the two slip planes, symmetrically oriented to the crack plane and inclined at 70.5° to the crack plane (direction of maximum shear stress for mode I cracks). The initial source position (x_0) along the slip plane is chosen to be at $4b$, where b is the magnitude of Burgers vector based on a previous study (Roberts et al. 2002). As the load is increased, dislocations are emitted and the crack-tip is blunted. The radius of the blunted crack ρ is taken to be equal to $N\ b\ \sin\alpha$, where N is the number of emitted dislocations, and α is the slip plane angle. As blunting increases: (a) the crack tip fields are modified to that of a blunted crack (b) source positions are chosen to be equal to the crack-tip radius, (i.e. $x_0 = \rho$), and (c) the notional crack-tip from which the image stress of dislocations is calculated is moved back to the center of curvature of the blunted crack. The distribution of microcracks obtained in the previous stage is placed ahead of the macrocrack on the crack plane beyond a distance $X_{\min} = 10$ μm (i.e. is about a grain diameter). At each time step, the stress ahead of the crack at distances X_p's (the microcracks are assumed to be at these positions) along the crack plane are calculated. Fracture is assumed when the tensile stress (σ^p_{yy}) at any of the particles (at distance X^i_p) reaches σ^i_F. When at any of the particles, $\sigma^p_{yy} \geq \sigma^i_F$ the simulation stops; and the applied load at the macrocrack determines the fracture toughness (K_F).

We used 12 different distributions of microcracks for each friction stress; here we report the results obtained for friction stress values from 200 to 600 MPa at intervals of 50 MPa. The friction stress values are then related to temperature using the Zerili–Armstrong relation (1987). Figure 4a shows the calculated fracture toughness with increasing temperature, the applied stress intensity K required for the tensile stress at X^i_P to reach the critical value σ^i_F increases rapidly at higher temperature. The factors that lead to this rapid increase are the decrease in the tensile stress at the microcrack due to crack-tip blunting and the increasing effects of the stress field (predominantly compressive) from emitted dislocations. These effects are more evident from Fig. 4b and c, where the number of emitted dislocations (N_F) and plastic zone size (d_F) for each friction stress at fracture ($K\text{-}applied = K_F$) are shown. The plastic zone size is the distance measured along the slip plane of the farthest dislocation from the crack-tip. This rapid increase in the fracture toughness corresponds to the transition from brittle to ductile behavior.

3.4 Origin of scatter in fracture toughness

Figure 5a shows the scatter of the radius of microcracks that leads to fracture (critical microcrack length). It should be noted that the critical microcrack size in all cases is around 2–3 μm, and that the scatter in these values is "very narrow" compared to size range of microcracks we considered. The scatter is also independent of temperature, which is consistent with experimental findings (Bowen et al. 1987). Figure 5a clearly shows that the critical microcrack size range (2–3 μm), is at the tail of the size distribution function

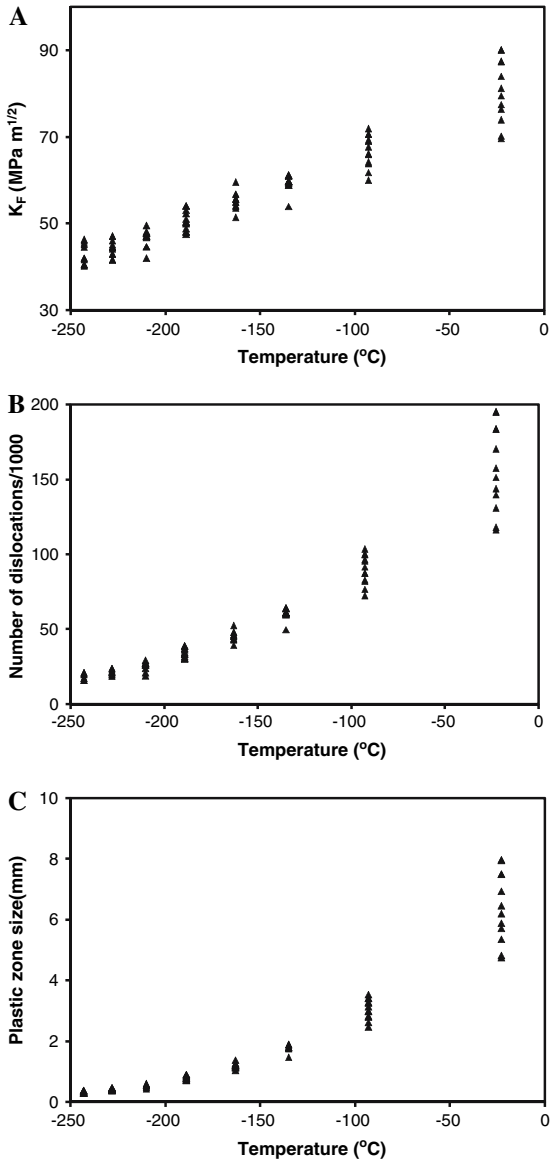

Fig. 4 (**a**) The fracture toughness (K_F) as a function of temperature stress for cases with six different microcrack configurations. The mean value curve is also shown. (**b**) The number of emitted dislocations as a function of temperature for six different microcrack configurations. (**c**) The plastic zone size (d_F) calculated at K_F as a function of temperature

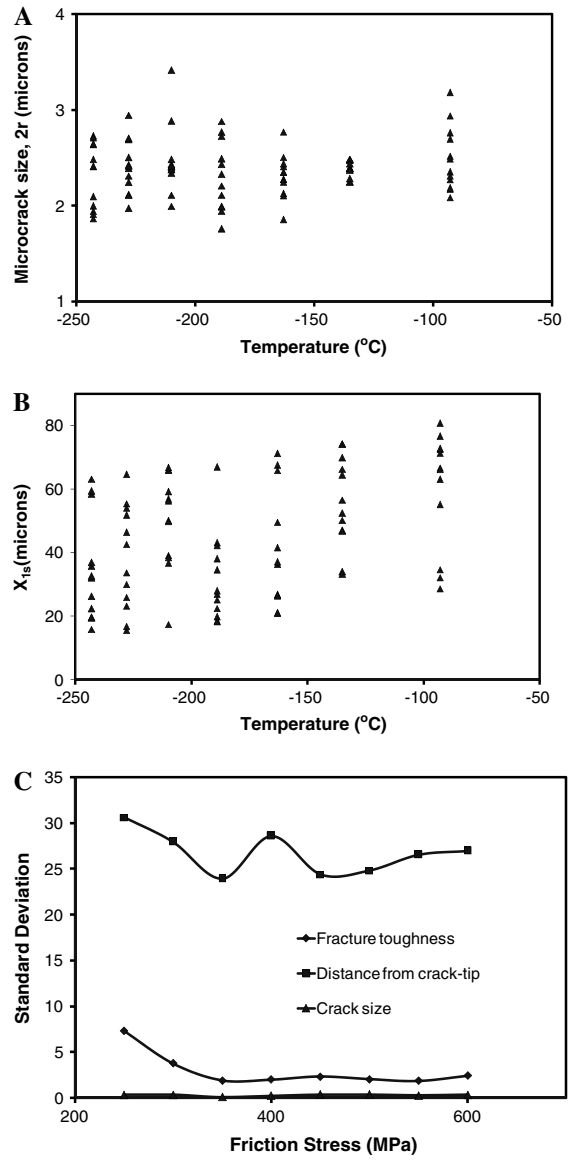

Fig. 5 (**a**) Temperature dependence of the critical microcrack size. (**b**) Temperature dependence of the critical microcrack distance from the main macrocrack tip. (**c**) Dependence of the relative standard deviations in K_F, a, and X_P on the friction stress

shown in Fig. 3. However it should be noted that the distance of these microcracks from the macrocrack-tip varies substantially from case to case, and is widely scattered as can be seen in Fig. 5b. Even though X_p is widely scattered, it is found that it is not correlated with the scatter in value of calculated K_F (compare Figs. 4a and 5b); whereas it appears that the critical micro crack size distribution is correlated with K_F (compare Figs. 4a and 5a) narrow. This can be further confirmed from Fig. 5c, where the relative standard deviation in a, X_p and K_F, is shown as a function of the friction stress. It can be seen that with friction stress the variation of standard deviation of K_F and a are similar; whereas that of K_F and X_P are not correlated. At Fig. 6, a detailed look at a typical fracture toughness data

(corresponding to a temperature of −189°C; friction stress = 450 MPa), further emphasizes this observation. Figure 6a shows the dependence of the fracture toughness on the critical microcrack size. Figure 6b shows fracture toughness values versus the position of the critical microcrack from the center of the blunted macrocrack. It is concluded from these simulations that the size of the microcrack has a strong correlation with the fracture toughness while its distance from the macrocrack tip is evidently not correlated with the fracture toughness.

3.5 Weibull analysis of the fracture toughness data

Here we follow earlier analyses of the fracture process in ferritic steels on the basis of the weakest-link theory (Wallin 1984). Consider the three-parameter Weibull model for probability of failure, given by

$$P_{\mathrm{f}} = 1 - \exp\left\{-\left[\frac{K_F - K_c}{K_0 - K_c}\right]^m\right\} \tag{2}$$

where P_{f} is the probability of failure, K_F is the toughness; K_0 a characteristic or scale value (63.2% of K_F lie below K_0). K_c is the guaranteed value or cut-off value below which fracture does not occur. The Weibull modulus m is a material parameter and should only depend on the size distribution of microcracks (see Appendix). The Weibull parameters obtained from our analysis for different temperatures are tabulated in Table 1. As expected, the Weibull modulus m is insensitive to temperature, it is found that m is in the range 1.3–3.4; note we used microcrack size distributions with the same mean properties for each temperature.

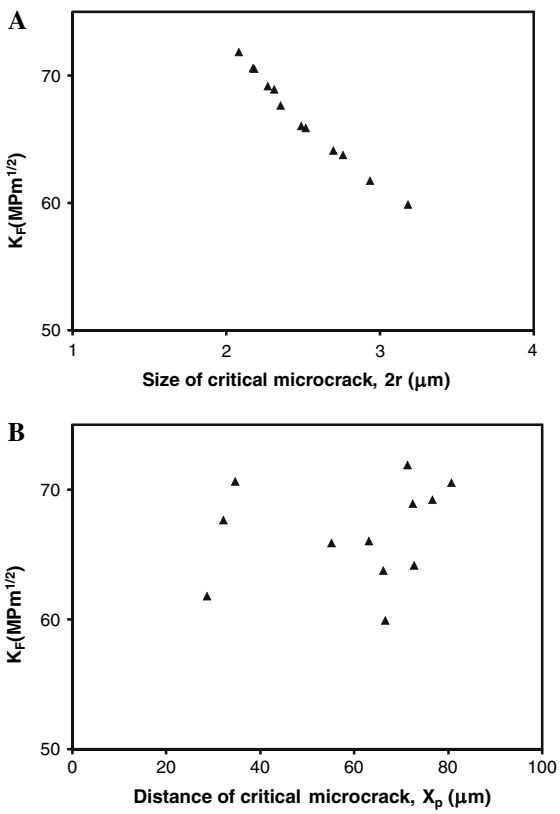

Fig. 6 (**a**) The dependence of the fracture toughness K_F, on the critical microcrack size for τ_y = 300 MPa. (**b**) Dependence of the fracture toughness K_F, on the distance of the critical crack from the main macrocrack for τ_y = 300 MPa

4 Conclusions

Earlier attempts to incorporate the weakest link theory in the fracture analysis of ferritic steels have assumed that the position of critical microcrack with respect to the macrocrack is the main source of data scatter in fracture toughness (Anderson et al. 1994). Our simulation results contradicts this view or assumption. We vividly demonstrate that the scatter in the fracture toughness arises from the scatter in the size of critical microcracks that lead to fracture. Moreover, the Weibull modulus was taken to be 4, and a fixed value of the size of the microcrack is used (Wallin 1984). In addition, plastic work during crack propagation was estimated from fits to experimental data. In the present model we explicitly account for the plastic work associated with dislocation emission, crack-tip shielding by emitted dislocation, and crack-tip blunting. Using a size distribution of microcracks, our calculated Weibull modulus is found to be lower and in the range of 1.3–3.4, consistent with the experimental observations.

The two-dimensional dislocation simulation used here does not explicitly account for dislocation climb, multiplication and hardening due to the interaction between dislocations. These processes may be more significant at higher temperatures. However the operation of dislocation sources in the present model is harder as dislocations are emitted due to an

Table 1 Weibull parameters estimated from fracture toughness calculations at different temperatures

Friction stress (MPa)	Temperature (°C)	Weibull modulus (m)	K_0 (MPa$\sqrt{}$m)	K_c (MPa$\sqrt{}$m)
600	−243	1.374	43.104	40.054
550	−228	2.405	45.187	40.428
500	−210	2.133	46.625	40.514
450	−189	1.445	50.100	47.045
400	−163	1.873	56.121	51.595
350	−130	2.949	59.891	52.892
300	−83	3.393	66.922	54.493
250	−3	2.116	82.491	65.545

The modulus m is a measure of the scatter of the data. K_0 is a characteristic value, and K_c is the guaranteed value

increasing back stress. Also crack-tip blunting results in geometric hardening which reduces the stress at dislocation source positions. Also, it should be noted that the dislocation density and plastic zone size obtained in our model at high temperature is well model still captures the sharp transition in fracture toughness at the brittle–ductile transition temperature.

Acknowledgements Support by the U S Department of Energy, Office of Fusion and Nuclear Energy through Grants DE-FG02-03ER54708 and DE-FC07-06ID14748 are gratefully acknowledged.

Appendix

To estimate the three parameters in Eq. 2 we proceed as follows: the fracture toughness (K_F) estimated numerically from our model is first ranked in an ascending order. The range of data is then divided into four equal classes and a histogram of probability density function (PDF) f is plotted. (The class value is represented by the mean of this range.) The density f of the class is the number of K_F in the ith class n_i divided by the product of the sample N and the class width w. The cumulative density function (CDF) is the area under the histogram up to the class,

$$P_{\mathrm{i}}(K_F) = \frac{f_i w_i}{2} + \sum_{j=1}^{i-1} f_j w_j \tag{A1}$$

where w_i is the width of the class with rank i and probability density f_i. At first, we assume $K_c = 0$; then from the plot of $\ln\ln(1/1 - P)$ versus $\ln(K_F/K_0)$ (see e.g. Fig. A1) then, we can estimate K_c as follows.

We first locate three points A, B, C such that they are equally spaced along the ordinate or $\ln\ln(1/(1-P))$ axis, thus by construction, we have

$$P_2 - P_1 = P_3 - P_2 = d \tag{A2}$$

or the displacements from origin are given as

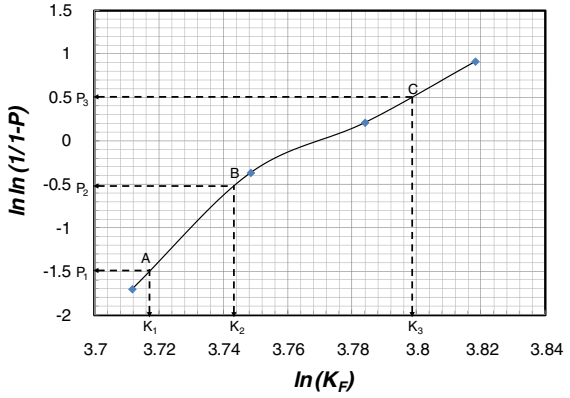

Fig. A1 $\ln\ln(1/(1-P))$ versus $\ln(K_F)$ for determination of K_c for the case of friction stress τ_y = 600 MPa, the points; note that $P_3-P_2 = P_2-P_1$

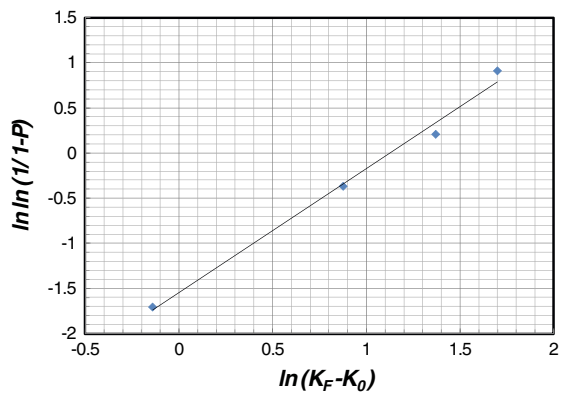

Fig. A2 $\ln\ln(1/(1-P))$ versus $\ln(K_F-K_c)$ for a friction stress τ_y = 600 MPa

$$P = S_P \ln \ln(1/1 - P) \tag{A3}$$

$$K = S_K \ln(K_F - K_c/K_0 - K_c). \tag{A4}$$

Taking the logarithm twice of Eq. 2 yields

$$\ln\left[\ln\left(\frac{1}{1-P}\right)\right] = m\ln(K_F - K_c) - m\ln(K_0 - K_c) \tag{A5}$$

Now substituting the (A3) (A2), we obtain,

$$K_c = K_2 - \frac{(K_3 - K_2)(K_2 - K_1)}{(K_3 - K_2) - (K_2 - K_1)} \tag{A6}$$

Now we compute a new set of data points using $(K_F - K_c)$ and replot $\ln\ln(1/(1-P))$ (see Fig. A2). The curve becomes linear implying that the data is indeed Weibullian. The slope of this line gives the Weibull modulus and the characteristic value (K_0) can be obtained from the value of $\ln(K_F - K_c)$ corresponding to $\ln\ln(1/(1-P))$.

References

Anderson, T.L., Stienstra, D., Dodds, R.H. Jr.: Theoretical framework for addressing fracture in the ductile-brittle transition region. In: Landes, J.D., McCabe, D., Boulet, J.A.M. (eds.) Fracture Mechanics: Twenty-fourth Volume, pp. 186–214. ASTM Philadelphia, PA, STP 1207 (1994)

Beremin, F.M.: Local criterion for cleavage fracture of a nuclear pressure vessel steel. Metall. Trans. **14**, 2277–2287 (1983)

Bowen, P., Druce, S.G., Knott, J.F.: Effects of microstructure on cleavage fracture in pressure vessel steel. Acta Metall. **35**, 1121–1131 (1987)

Chen, J.H., Chu, L., Wang, G.Z., Wang, Z.: Further investigation of critical events in cleavage fracture of C-Mn base and weld steel. Metall. Trans. A **24**, 659–667 (1993)

Curry, D.A., Knott, J.F.: Relationship between fracture toughness and microstructure in the cleavage fracture of mild steel. Metal Sci. **10**, 1–6 (1976)

Curry, D.A., Knott, J.F.: Effects of microstructure on cleavage fracture stress in steel. Metal Sci. **12**, 511–514 (1978)

Curry, D.A., Knott, J.F.: Effect of microstructure on cleavage fracture toughness of quenched and tempered steels. Metal Sci. **13**, 341–345 (1979)

Hirsch, P.B., Roberts, S.G.: Modelling crack tip plastic zones and the brittle-ductile transition. Phil. Trans. R. Soc. Lond. A. **355**, 1991–2001 (1997)

Jayatilaka, A.DeS., Trustrum, K.: Statistical approach to brittle fracture. J. Mater. Sci. **12**, 1426–1430 (1977)

Knott, J.F.: The Micro-mechanisms of Fracture in Steels used for high integrity structural components. In: Hirsch, P.B., Lidbury, D. (eds.) Fracture, Plastic Flow and Structural Integrity, pp. 21–43. IOM Communications Ltd, London (2000)

McMahon, C.J. Jr., Cohen, M.: Initiation of cleavage in polycrystalline iron. Acta Metall. **13**, 591–604 (1965)

Noronha, S.J., Ghoniem, N.M.: Brittle-ductile transition in F82H and effects of irradiation. J. Nucl. Mater. **367–370**, 610–615 (2007)

Ortner, S.R., Hippsley, C.A.: Two component description of ductile to brittle transition in ferritic steel. Mater. Sci. Technol. **12**, 1035–1042 (1996)

Poloniecki, J.D., Wilshaw, T.R.: Glass surface cracks-Hertzian fracture data and a new analytical method. Nat. Phys. Sci. **229**, 226–227 (1971)

Press, W.H., Teukolsky, S.A., Vellerling, W.T., Flannery, B.P.: Numerical Recipies. Cambridge University Press (1996)

Roberts, S.G., Noronha, S.J., Wilkinson, A.J., Hirsch, P.B.: Modelling the initiation of cleavage fracture of ferritic steels. Acta Mater. **50**, 1229–1244 (2002)

Wallin, K.: Scatter in KI_c-results. Eng. Fract. Mech. **19**, 1085–1093 (1984)

Wallin, K., Saario, T., Törrönen, K.: Micromechanism based statistical model for brittle fracture. Metal Sci. **18**, 13–16 (1984)

Zerilli, F.J., Armstrong, R.W.: Dislocation-mechanics-based constitutive relations for material dynamics calculations. J. Appl. Phys. **61**, 1816–1825 (1987)